Oscillation of Supersonic Inflatable Aerodynamic Decelerators at Mars

AE8900 MS Special Problems Report
Space Systems Design Lab (SSDL)
Guggenheim School of Aerospace Engineering
Georgia Institute of Technology
Atlanta, GA

Author:
Brandon P. Smith

Advisors:
Robert D. Braun
Ian G. Clark

17 December 2010

Oscillation of Supersonic Inflatable Aerodynamic Decelerators at Mars

Brandon P. Smith[1], Ian G. Clark[2], Robert D. Braun[3]
Georgia Institute of Technology, Atlanta, GA, 30332-0150

This analysis considers the dynamic stability of a notional Mars 2018 entry probe augmented with an attached supersonic inflatable aerodynamic decelerator (SIAD) deployed at Mach 5. Dynamics of the attached isotensoid and tension cone SIAD configurations are compared using an explicit solution to the planar equations of motion. A current experimental database of flexible isotensoid and tension cone static aerodynamics is employed in the simulation. Pitch-damping data from the Mars Science Laboratory (MSL) ballistic range tests is parameterized and applied to the SIAD-augmented portion of flight. The Mach number at which safe parachute deployment can occur depends on the amplitude of pitch oscillation, so the sensitivity of this metric to the parameterized pitch-damping behavior is determined. Pitch dynamics yielding unacceptable parachute staging conditions are quantified to inform SIAD configuration selection and design. These exploratory results are used to recommend a general strategy for measuring the pitch dynamics of SIAD-augmented blunt vehicles in ground testing facilities.

Nomenclature

A	=	Cauchy-Euler coefficient
B	=	oscillation coefficient driving pitch damping
C	=	oscillation coefficient driving pitching frequency
C_A	=	aerodynamic axial force coefficient
C_N	=	aerodynamic normal force coefficient
C_D	=	aerodynamic drag coefficient
C_L	=	aerodynamic lift coefficient
C_{L_α}	=	aerodynamic lift-slope coefficient
C_{m_α}	=	aerodynamic pitching-moment slope coefficient
$C_{m_q}+C_{m_{\dot\alpha}}$	=	aerodynamic pitch-damping sum
C_{m_q}	=	aerodynamic pitch-damping coefficient
$C_{mq,max}$	=	maximum pitch-damping coefficient parameter
d	=	aerodynamic reference diameter: diameter of aeroshell or SIAD
h	=	altitude above planet's equatorial radius
I_{yy}	=	pitch-axis mass moment of inertia
g	=	acceleration due to gravity (Mars: 3.71 m/s^2)
m	=	total vehicle mass including decelerator
M	=	Mach number
$M_{\alpha=10^\circ}$	=	Mach number where $\lvert\alpha\rvert$ exceeds 10º
R_p	=	planet equatorial radius (Mars: 3,396 km)
S	=	aerodynamic reference area, $\pi d^2/4$

[1] Graduate Research Assistant, Daniel Guggenheim School of Aerospace Engineering, AIAA Member.
[2] Visiting Assistant Professor, Daniel Guggenheim School of Aerospace Engineering, AIAA Member.
[3] Associate Professor, Daniel Guggenheim School of Aerospace Engineering, AIAA Fellow.

t = time
V = atmosphere relative velocity
$\vec{x}$ = angle-of-attack state vector
x_{cg} = longitudinal distance between aeroshell nose and center of gravity

Greek

$\Delta Mach$ = Mach number shift parameter
$\Delta\alpha$ = angle-of-attack shift parameter
α = angle-of-attack
γ = flight path angle
δ = Cauchy-Euler phase shift
ζ = damping ratio
λ = pitch-damping coefficient linear scaling parameter
μ = Cauchy-Euler decay exponent
ν = Cauchy-Euler frequency term
ρ = atmospheric density
ω_n = undamped natural frequency

Subscripts

i = initial quantity
ISO = isotensoid quantity
MSL = Mars Science Laboratory quantity
SIAD = combined aeroshell and supersonic inflatable aerodynamic decelerator quantity
TC = tension cone quantity

I. Introduction

Deployable supersonic inflatable aerodynamic decelerators (SIADs) provide a means to greatly increase the drag of a planetary entry vehicle with little mass penalty. At Mars, SIADs attached to blunt bodies have been shown to greatly increase landed mass capability, enable landing at higher altitudes, enable other key planetary descent technologies, and provide mass-growth robustness during system design.[1] Although the static aerodynamic performance of favored configurations is well understood[2,3], little work exists that considers the dynamic motion characteristics of blunt bodies with attached SIADs. Furthermore, the stability derivatives for SIADs have never been measured experimentally. Obtaining such data is necessary prior to selection of a SIAD as a deployable decelerator at Mars because simulations of SIAD-aeroshell oscillatory motion may limit the staging conditions for a supersonic or subsonic parachute. Additionally, a general lack of confidence in common SIAD parametric mass estimation methods hinders selection of one configuration over another based only on mass considerations. Consequently, selecting a suitable SIAD configuration may be dictated by oscillatory motion characteristics.

Blunted large-angle cones are a common aeroshell choice for planetary probe missions requiring high aerodynamic drag and low aerothermal heating. Unfortunately, these shapes exhibit oscillation growth during deceleration from hypersonic continuum conditions to subsonic conditions. Blunted large-angle cones are statically stable through the majority of these flow regimes though may exhibit static instability at some conditions with angles-of-attack less than 2°.[4,5] The oscillations are caused by a bounded dynamic instability that occurs in blunt bodies during deceleration through the high supersonic flow regime and continues to grow as speeds decelerate through transonic and subsonic flight. Dynamic instabilities thought to stem primarily from wake flow interactions with the vehicle aftbody are the mechanism for pitch and yaw oscillation amplitude growth. In subsonic flow these dynamic instabilities can overwhelm the static restoring moment and induce an uncontrollable tumbling motion.[6] Figure 1 shows example pitch-damping coefficient results as a function of Mach number and angle-of-attack from the Mars Science Laboratory (MSL) ballistic range tests.[7] These results show that lower Mach numbers experience dynamic instabilities at larger angles-of-attack resulting in prevalent limit-cycle oscillations.

Recognizing the complete lack of dynamic stability data for the favored SIAD configurations, Musil[8,9] applied empirical blunt-body stability derivatives to SIADs in a comprehensive Viking-era SIAD system study for NASA Jet Propulsion Laboratory. Although the work calls out several approximations that caveat the use of blunt-body stability derivatives for flexible structures, the results show the importance of considering dynamic motion characteristics as discriminators when down-selecting SIAD configurations. Axdahl[10] studied the dynamics of a SIAD by developing a simulation framework to predict the stability behavior for the entry vehicle based on interface stiffness and damping parameters. The pitch-damping coefficient was computed with a modified Newtonian method

and assumed invariant with angle-of-attack. This foundational work was the first to consider the impact of a flex-interaction mode between a SIAD and the rigid aeroshell. The current analysis builds on prior work by approaching the problem as one of trajectory design. It will be shown that the results of this analysis are complementary to the past work and together provide a framework for interpreting future SIAD dynamic stability data.

The two foremost SIAD configurations are considered in this study of SIAD oscillations: the attached isotensoid and tension cone. Photographs of notional configurations are provided in Fig. 2. Fortunately, a comprehensive set of experimental static aerodynamics from subsonic to high supersonic conditions exists for flexible configurations of both SIADs. Furthermore, it is expected that SIADs will exhibit similar dynamic behavior to traditional blunt-body entry vehicles (i.e. oscillation growth from supersonic speeds through subsonic speeds). Additionally, the supersonic inflation event introduces a short period of time where the precise aerodynamic shape is uncertain and aerodynamic coefficients cannot be meaningfully predicted. In the absence of SIAD pitch-damping knowledge, it is necessary to explore the dynamic behavior of the SIAD-aeroshell system using simulated data.

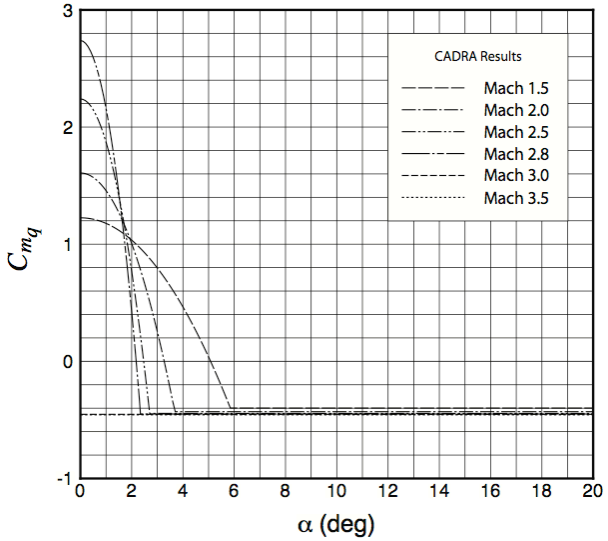

Figure 1. MSL 70º sphere-cone pitch-damping behavior: data reduced using the AerospaceComputing Inc. CADRA code.[7] Positive pitch-damping coefficients represent dynamic instability.

This analysis considers the dynamic stability of a notional Mars 2018 entry vehicle augmented with an attached SIAD deployed at Mach 5. The research builds on the past literature by characterizing the dynamics of the SIAD-aeroshell system from pre-deployment hypersonic conditions through subsonic conditions. An explicit solution to the planar equations of is developed. Angle-of-attack histories are computed from an initial state at Mach 6 through SIAD deployment and subsequent deceleration to subsonic speeds. Current databases of flexible tension cone and isotensoid experimental static aerodynamics are used. Pitch-damping data from ballistic range and forced oscillation test data of a representative blunt body is generalized for the trajectory analysis. Allowable Mach number lower-bounds for both SIAD configurations are computed based on the Mars Phoenix aeroshell parachute deployment state requirements. Pitch dynamics yielding unacceptable staging conditions are quantified to inform SIAD configuration selection and design. Finally, the trajectory analysis is used to suggest experimental techniques for obtaining the required pitch-damping data using ground test facilities.

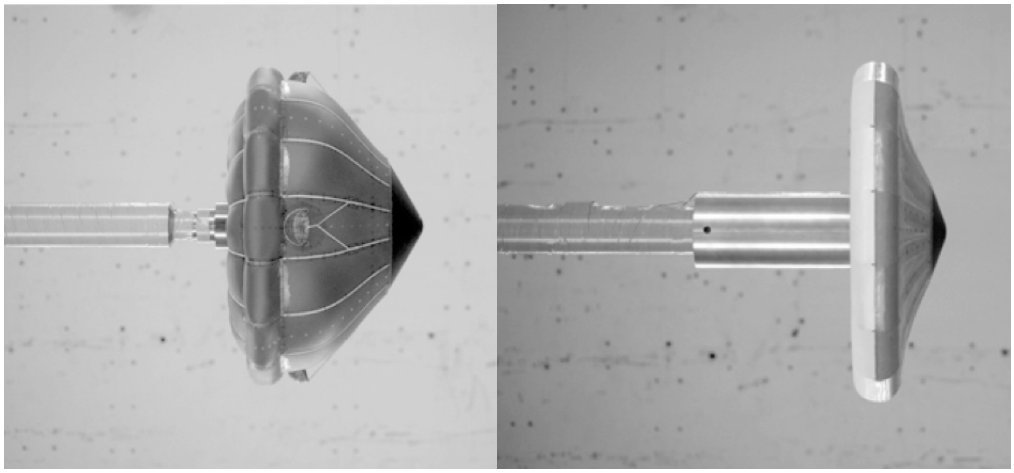

Figure 2. Photographs of the attached isotensoid (left) and tension cone (right) SIADs during a transonic wind tunnel test at the NASA Langley Transonic Dynamics Tunnel (TDT).[3]

II. Modeling

A. Reference Mission

This analysis considers a robotic Mars entry vehicle augmented with a SIAD deployed at Mach 5. A representative set of entry conditions for a 2018 Mars flight opportunity is considered. Flight conditions at Mach 6 are estimated based on correspondence and used as initial conditions in this trajectory simulation. The initial state is provided in Table 1. The flight path angle (γ) is considered negative when the velocity vector is oriented below the local horizon.

Table 1. Nominal initial flight conditions.

Parameter	Value
Mach number, M	6.0
Altitude, h	13.5 km
Flight path angle, γ	0º
Angle-of-attack, α	2º

B. Aeroshell Definition

A 70º sphere-cone aeroshell similar to those used for the Viking, Pathfinder, Mars Exploration Rovers (MER), Phoenix, and MSL aeroshells is considered for this representative Mars 2018 entry vehicle. In accordance with past mass growth trends, a larger and higher mass aeroshell than MSL is considered for this analysis. A comparison of MSL aeroshell properties and those used for this study is shown in Table 2. The MSL properties are representative of those at Mach 6 and after any center of gravity offset ballast meant to induce a non-zero trim angle-of-attack has been ejected.

Table 2. Aeroshell properties.

Parameter	MSL[7]	This Study
Sphere-cone angle, θ	70º	70º
Diameter, d	4.5 m	4.7 m
Mass (no SIAD)	3067 kg	3500 kg
I_{yy}	3353 kg-m^2	3800 kg-m^2
x_{cg}/d	0.3	0.3

C. Supersonic Inflatable Aerodynamic Decelerator Definitions

The attached isotensoid and tension cone have markedly different inflation schemes. The supersonic isotensoid configuration relies on a separate energy source to expose the SIAD envelope fabric enough such that one or more of the ram-air inlets "catch" the surrounding flow. Ram-air inflates the SIAD envelope until a maximum internal pressure is reached. Several isotensoid deployments in supersonic wind tunnels have shown that the internal pressure of the isotensoid reaches a maximum near twice the freestream dynamic pressure.[11,12] Conversely, the inflation pressure requirements for tension cones are driven by torus buckling concerns.[1] The inflation pressure required to maintain the tension cone shape in a supersonic flow field is far greater than what could be captured with ram-air techniques, so gas generators must provide enough torus pressure throughout the trajectory to sustain the dynamic pressure load and prevent bucking.

The SIAD in this analysis is designed to achieve a supersonic drag area (C_DA) approximately four times higher than the rigid aeroshell alone. This yields a target C_DA of 105 m^2 and corresponding SIAD diameters of approximately 11 meters for the isotensoid and 9.5 meters for the tension cone. Mass and pitch-axis mass moment of inertia for stowed and deployed configurations are estimated in Table 3. The stowed isotensoid mass is taken from an 11 meter diameter flight article constructed for a subsonic helicopter drop test by NASA Langley in the late 1960s.[13] The increase in mass for the inflated isotensoid is estimated by assuming the internal stagnation air inside the canopy is a perfect gas at a pressure equivalent to twice the dynamic pressure of the freestream flow.[11,12] Tension cone mass estimates come from the method described by Clark and include the mass of the gas generators.[1] Stowed moments of inertia are estimated by assuming the SIAD is stored in a ring located near the aeroshell shoulder. Inflated moments of inertia are estimated by assuming the SIAD approximates an inertial ring located at the tension cone torus's radial distance and the isotensoid's cross-section centroid.

Table 3. SIAD estimated mass properties.

Parameter	Stowed	Inflated
m_{ISO}	36 kg	42 kg
$I_{yy,ISO}$	104 kg-m^2	218 kg-m^2
m_{TC}	40 kg	40 kg
$I_{yy,TC}$	116 kg-m^2	420 kg-m^2

SIAD inflation changes the entry vehicle's static aerodynamic forces and moments, aerodynamic damping, and mass distribution. All three of these changes may influence the pitch dynamics of the entry vehicle. In order to capture the main effects of inflation, a linear interpolation of stowed and deployed SIAD mass and diameter is employed. Nominal inflation duration is prescribed as one second.

D. Simulation Methodology

The oscillatory motion of the aeroshell and attached SIAD systems are computed through numerical integration of the governing equations. The mission parameters described in Tables 1-3 provide the needed inputs to simulate the trajectory by propagating forward in time from an initial state. The physics of this problem can be decomposed according to the design structure matrix (DSM) shown in Fig. 3. Interdependencies of the models are detailed by showing which parameters are passed through feedback and feedforward loops. Prior to SIAD deployment, the DSM includes a model that provides the aerodynamics of the aeroshell alone. After SIAD deployment, the DSM instead includes a model that provides aerodynamics and mass properties of the aeroshell with the attached SIAD.

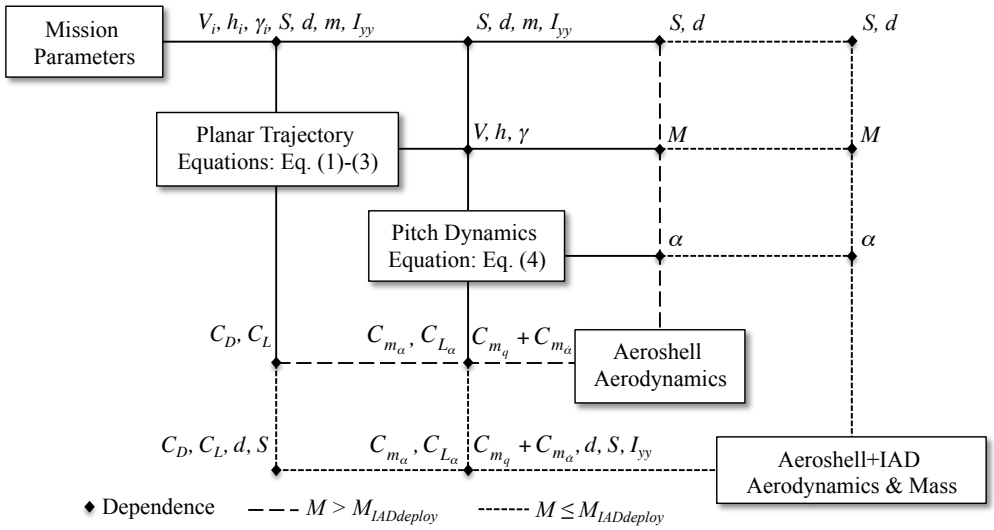

Figure 3. Pitch dynamics simulation framework showing interdependencies.

E. Equations of Motion

The planar equations of motion for an entry vehicle descending through an atmosphere are shown below in Eq. (1) through Eq. (3).[14] These relations are valid for entry vehicles with low lift-to-drag ratios.

$$\frac{dV}{dt} = -\frac{\rho V^2 S C_D}{2m} - g\sin\gamma \tag{1}$$

$$\frac{d\gamma}{dt} = \frac{\rho V S C_L}{2m} - \left(\frac{g}{V} - \frac{V}{R_e + h}\right)\cos\gamma \tag{2}$$

$$\frac{dh}{dt} = V \sin\gamma \tag{3}$$

Resolving angular motion of the entry vehicle requires additional information about the vehicle mass (m), pitch-axis moment of inertia (I_{yy}), static aerodynamics (C_{L_α}, C_{m_α}), and pitch-damping sum ($C_{m_q} + C_{m_{\dot\alpha}}$). Schoenenberger[15] develops a general equation for the planar pitching motion of a re-entry vehicle over a trajectory segment where the vehicle is traveling much faster than its terminal velocity or is traveling at a small flight path angle:

$$\ddot\alpha - \frac{\rho VS}{2m}\left(-C_{L_\alpha} + \frac{md^2}{2I_{yy}}\left(C_{m_q} + C_{m_{\dot\alpha}}\right)\right)\dot\alpha - \frac{\rho V^2 Sd}{2I_{yy}} C_{m_\alpha}\alpha = 0 \tag{4}$$

Pitch-damping effects from the two constituent terms in the pitch-damping sum, C_{m_q} and $C_{m_{\dot\alpha}}$, are generally not distinguishable in flight above transonic speeds. Cross flows are much slower than translational flows at supersonic and hypersonic speeds, so there is essentially zero flow-lag to distinguish the two constituent terms of the pitch-damping sum. Nevertheless, short-period pitch damping in the flow regimes of interest can be evaluated satisfactorily if the combined pitch-damping sum is known.[14,16] The pitch-damping sum measured in experiment is often truncated and written only as the pitch-damping coefficient. Such is the case in this analysis.

Equation (4) is a second-order damped harmonic oscillator with time-dependent coefficients. An analytic solution to Eq. (4) is available by assuming constant density (ρ), flight path angle (γ), aerodynamic derivatives (C_{L_α}, C_{m_α}, $C_{m_q} + C_{m_{\dot\alpha}}$), reference dimensions (S, d), and mass properties (m, I_{yy}).[15] These assumptions are suitable for modeling pitching behavior of blunt bodies in ground test facilities. However, simulating free-flight behavior of an entry vehicle deploying a SIAD and decelerating to subsonic conditions precludes use of these analytic methods. An explicit numerical solution to Eqs. (1)-(4) is developed here to compute the angle-of-attack history through the entire trajectory. To begin, the planar trajectory equations are solved using a simple Euler method. Given an initial state, these ordinary differential equations lend themselves to rapid computation of the planar trajectory. It is assumed that the angle-of-attack oscillation has negligible effect on the velocity, flight path angle, and altitude profiles. That is, the planar trajectory is solved assuming static aerodynamics at zero angle-of-attack. The planar trajectory data is then used to solve for the angle-of-attack history given an initial angle-of-attack tip-off condition at Mach 6. To begin, Eq. (4) is recast in a more tractable form:

$$\ddot\alpha + B\dot\alpha + C\alpha = 0 \tag{5}$$

where

$$B = -\frac{\rho VS}{2m}\left(-C_{L_\alpha} + \frac{md^2}{2I_{yy}}\left(C_{m_q} + C_{m_{\dot\alpha}}\right)\right) \tag{6a}$$

and

$$C = -\frac{\rho V^2 Sd}{2I_{yy}} C_{m_\alpha} \tag{6b}$$

Equation (5) can be solved in MATLAB using an explicit Runge-Kutta method (ode45). This method efficiently solves systems of first-order non-linear ordinary differential equations. Equation (5) is a second-order non-linear ordinary differential equation, so we must first reduce the order to use the MATAB functionality. The angle-of-attack and its time derivatives can be written in vector form by defining a new vector variable $\vec{x}$:

$$\vec{x} = \begin{bmatrix} x_1 \\ x_2 \end{bmatrix} = \begin{bmatrix} \alpha \\ \dot{\alpha} \end{bmatrix} \tag{7}$$

Differentiating with respect to time, it follows that

$$\dot{\vec{x}} = \begin{bmatrix} \dot{x}_1 \\ \dot{x}_2 \end{bmatrix} = \begin{bmatrix} \dot{\alpha} \\ \ddot{\alpha} \end{bmatrix} \tag{8}$$

Thus, Eq. (5) can be written as a first-order vector ordinary differential equation:

$$\begin{bmatrix} \dot{x}_1 \\ \dot{x}_2 \end{bmatrix} = \begin{bmatrix} 0 & 1 \\ -C & -B \end{bmatrix} \begin{bmatrix} x_1 \\ x_2 \end{bmatrix} \tag{9}$$

The coefficients B and C depend on known trajectory parameters, static aerodynamics (C_{L_α} and C_{m_α}), and the pitch-damping sum ($C_{m_q} + C_{m_{\dot{\alpha}}}$). Aerodynamic models for the aeroshell alone and SIAD-aeroshell systems are discussed in subsequent sections.

F. Static Aerodynamics

The 70º sphere-cone aeroshell lift and drag coefficients are derived from modified Newtonian flow relations using a code written by Grant.[17] Static stability data for the aeroshell is taken from the MER ballistic range results.[18] Flexible SIAD-aeroshell static aerodynamics are taken from a current experimental database compiled by Hill[19] from the published modern and historic wind tunnel test data for attached isotensoid and tension cone models. The static aerodynamic parameters influencing the pitch motion and ballistic trajectory are shown in Figure 4.

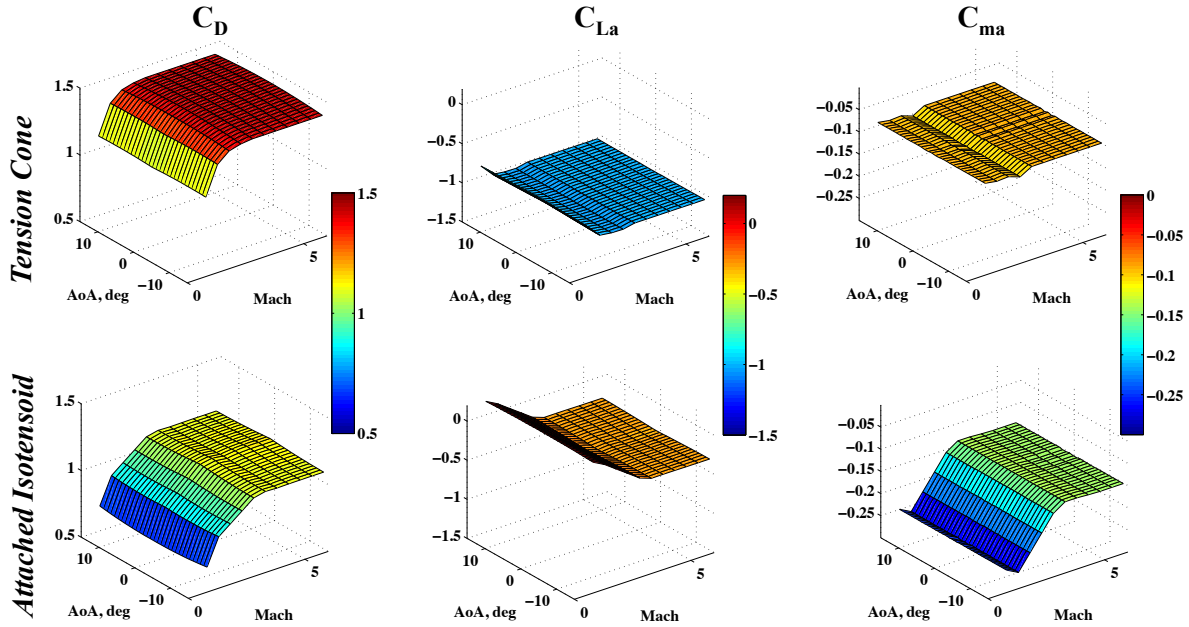

Figure 4. Tension cone and attached isotensoid static aerodynamics. The data used to generate these surfaces is compiled from published results of flexible-article wind tunnel tests.[19]

G. Dynamic Stability

Dynamic stability refers to the ability of a vehicle to damp oscillations induced by the static restoring moments when perturbed from steady flight. This analysis neglects motion about the yaw and roll axes, so the dynamic stability of the vehicle is solely a function of the pitch-damping characteristics. In particular, the pitch-damping coefficient must be known as a function of Mach number and angle-of-attack. Determining this quantity for atmospheric entry vehicles remains a challenging area of research. Pitch damping is thought to be a primarily a function of the unsteady near-wake flow inducing forces and moments about the aftbody. However, there is no clear understanding of the physical phenomena that leads to dynamic instability, and the experimental observations of blunt-body dynamic stability are often contradictory.[20-21] Computational fluid dynamics (CFD) codes known to provide highly accurate static stability information can also be used to compute pitch-damping derivatives, but there is a large computational cost due to the number of solutions required to generate a single pitch-damping estimate. Murman computed the pitch-damping coefficient for two blunt-body configurations using the NASA code Overflow and showed some agreement with experimental data by including the pitch-rate dependency of the pitch-damping coefficient.[22] In a related study of SIAD pitch damping, Murman compares the pitch damping of a rigid stacked-toroid blunted cone SIAD with a rigid tension cone SIAD. The tension cone is estimated to have a worst-case pitch-damping coefficient near 0.18 (occurs at Mach 2.5).[23] Note that this rigid-body analysis does not capture the SIAD-aeroshell flex-interaction mode. Others have had success computing pitch-damping coefficients of slender and blunt entry vehicle configurations using code-level modifications to three-dimensional Navier-Stokes solvers[24] or linearized characteristics methods[25]. Despite the progress in computational methods for predicting pitch damping, the American Mars entry vehicle missions have all used experimental data collected from the Viking[26], MER[18], and MSL[7] entry vehicle aerodynamic test programs to populate their dynamic stability databases.

This analysis uses results from the MSL ballistic range tests for the aeroshell pitch dynamics. This free-flight data was taken at the Aeroballistic Research Facility (ARF) at Eglin Air Force Base, Florida. A description of the ballistic range test technique is given later in this paper, but the results of the MSL test are discussed here. Two companies who developed their own parameter estimation software independently reduced the MSL ARF data.[7] The form of the pitch-damping coefficient versus Mach number versus angle-of-attack data is quite different between the two data reduction techniques, but the simulated pitch behavior seen when applying the curves is similar. This illustrates the inherent non-uniqueness of these parameter estimation methods: there is more than one possible form of the pitch-damping function that can reproduce the observed behavior. One company's results (Arrow Tech) were similar in form to the MER ballistic range results. The other company's results (AerospaceComputing) were of a very different functional form. Namely, they predicted a distinct Mach number (Mach 2.8) where dynamic stabilities arise at low angles-of-attack. These results were shown earlier in Fig. 1. Below Mach 2.8, the pitch-damping coefficient becomes positive (unstable) and much larger in magnitude over a short range of angle-of-attack. The instability becomes weaker as the vehicle decelerates but extends over a larger angle-of-attack region. This previously unseen functional form of the pitch-damping coefficient is not thought to arise from MSL-specific phenomena, but rather is an artifact of improved data reduction techniques and observations from the Crew Exploration Vehicle (CEV) forced-oscillation tests. To complete the aeroshell pitch-damping data set for this analysis, low Mach number pitch-damping data outside the bounds of the MSL tests are taken from a study by Mitcheltree[6]. The composite pitch-damping behavior assumed in this analysis for the aeroshell-only portion of flight is shown below in Fig. 5.

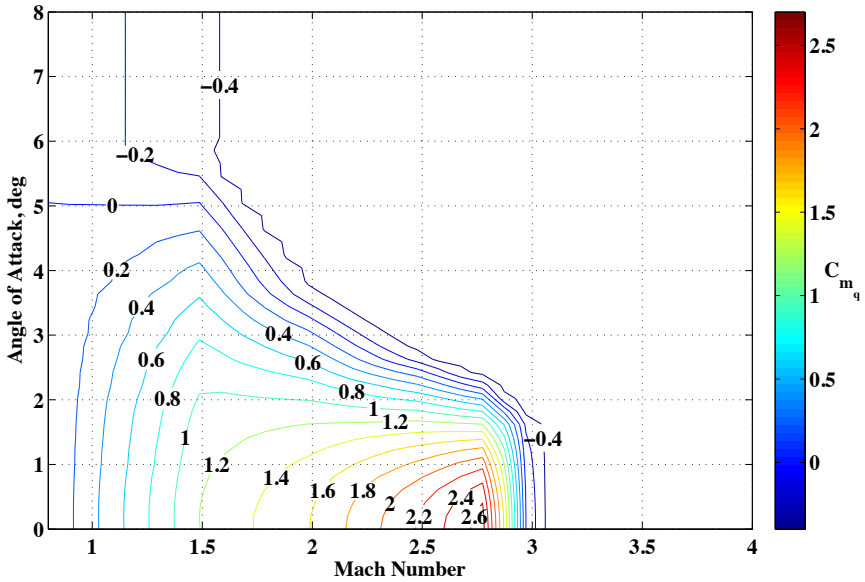

Figure 5. Composite pitch-damping data assumed for aeroshell-only portion of flight (adapted from Refs. 6 and 7).

The pitch-damping coefficients of flexible attached isotensoids and tension cones have not been measured. Past studies of SIAD pitch oscillation have applied blunt-body pitch-damping behavior to the SIAD-aeroshell phase of flight.[8,9] The analysis in this study builds on past work by exploring SIAD-aeroshell dynamic stability assuming the pitch-damping derivative is of the same functional form as the MSL ballistic range results reduced by AerospaceComputing. The experimental results from the MSL test series are believed to be the best-informed experimental observations of blunt-body dynamic stability available over the flight regime of interest. This approach allows the pitch-damping curve to be parameterized, and the sensitivity of the oscillatory behavior to the pitch-damping coefficient can be explored. Such results provide a quick resource for system-level interpretation of future SIAD dynamic stability experimental data. In particular, the lowest Mach number at which a supersonic parachute can be deployed is quantified as a function of the SIAD pitch-damping behavior.

III. Results

A. Simulation Validation

The explicit solution to Eq. (4) described above is validated using an analytic solution developed by Schoenenberger for a decelerating vehicle at constant altitude with linear static aerodynamics.[15] These conditions closely approximate flight in a ballistic range. Assuming a constant drag coefficient, the velocity over a limited time domain can be written as:

$$V = \frac{2m}{\rho S C_A t} \tag{10}$$

where C_A is the axial force coefficient. Substituting Eq. (10) into Eq. (4) and assuming small angle-of-attack ($C_{L_\alpha} \approx -C_A$) yields a Cauchy-Euler ordinary differential equation:

$$t^2\ddot{\alpha} - \left(1 + \frac{md^2}{2I_{yy}}\frac{C_{m_q} + C_{m_{\dot\alpha}}}{C_A}\right)t\dot{\alpha} - \frac{2m^2 dC_{m_\alpha}}{\rho S I_{yy} C_A^2}\alpha = 0 \tag{11}$$

The solution to this equation is known:

$$\alpha = At^\mu \cos\left(\nu \ln t + \delta\right) \tag{12}$$

where A and δ are determined from the initial conditions and μ and ν are given by:

$$\mu = \frac{md^2\left(C_{m_q} + C_{m_{\dot\alpha}}\right)}{4I_{yy}C_A} + 1 \tag{13}$$

and

$$\nu = \sqrt{-\frac{2m^2 dC_{m_\alpha}}{\rho S C_A^2 I_{yy}}} \tag{14}$$

Results from the explicit method and Cauchy-Euler analytic method are compared using the example ballistic range parameters in Ref. 15. The explicit method is able to recreate the analytic solution nearly perfectly for this case, as shown in Fig. 6 for three values of the pitch-damping sum. Furthermore, Schoenenberger verified the ability of the Cauchy-Euler solution to mimic the results of the Program to Optimize Simulated Trajectories (POST), a respected trajectory analysis tool used widely within NASA and industry.

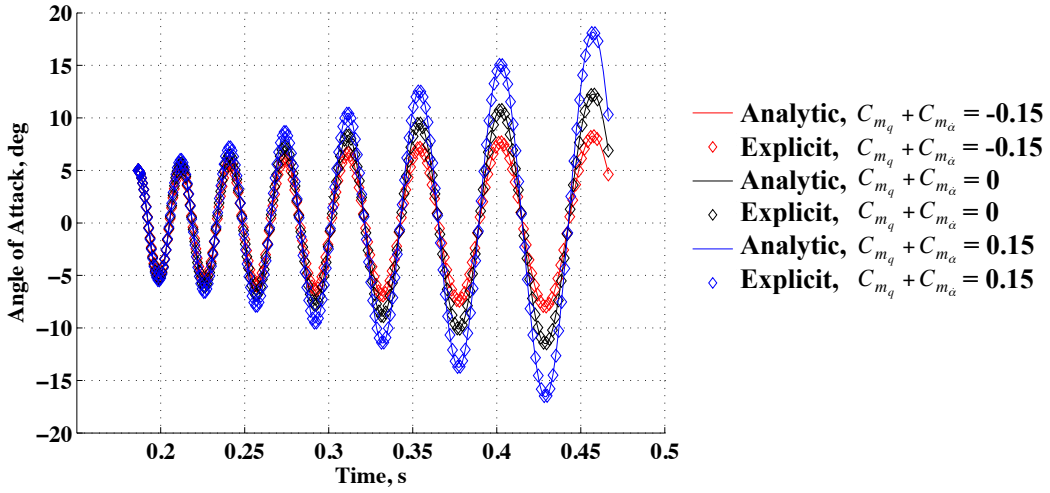

Figure 6. Validation of explicit method developed in this analysis with analytic Cauchy-Euler solution with parameters from Ref. 15.

It is useful examine the dynamic behavior when an aeroshell is decelerating unaided by a SIAD to see if the simulation agrees what has been observed in flight. Figure 7 shows the simulated angle-of-attack history for the MSL aeroshell during deceleration from Mach 6 to transonic speeds. As expected from the assumed pitch-damping behavior in Fig. 4, the motion becomes dynamically unstable at Mach 2.8 and oscillation amplitude growth is observed.

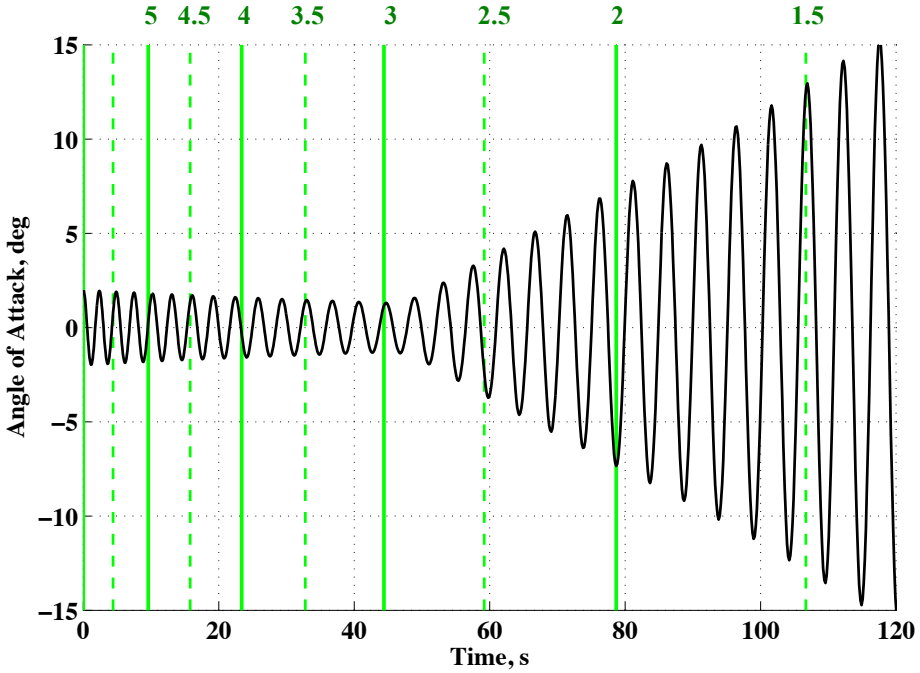

Figure 7. Simulated angle-of-attack history for the MSL aeroshell during deceleration from Mach 6. Vertical lines indicate Mach number.

MSL makes use of a reaction control system (RCS) that can easily counter any dynamic instability inherent to the aeroshell aerodynamics, so the motion shown in Fig. 7 will be not be seen in practice.[7] MSL is the first Mars mission that will use RCS for trajectory control during the entry phase. Earlier Mars missions have all deployed stabilizing parachutes before the angle-of-attack oscillation amplitude becomes too large. Pre-flight simulation of the Mars Pathfinder entry vehicle predicted a region of oscillation growth due to the supersonic dynamic instability region. Concerns over oscillation growth helped to set the required parachute deployment Mach number for this

mission. The reconstructed trajectory from data onboard the Pathfinder probe bears striking resemblance to pre-flight predictions. A comparison of the simulated and reconstructed Mars Pathfinder angle-of-attack history is shown in Fig. 8.

Note the MSL RCS consists of four pairs of reaction control jets located on the backshell. It is evident from the geometry of attached SIADs shown in Figure 1 that such a system would interfere with the flexible material. The fact that controlled flight with a SIAD may not be possible emphasizes the importance of high-fidelity knowledge of the flexible SIAD-aeroshell pitch damping. Such knowledge enables selection of a safe Mach number lower bound for parachute deployment.

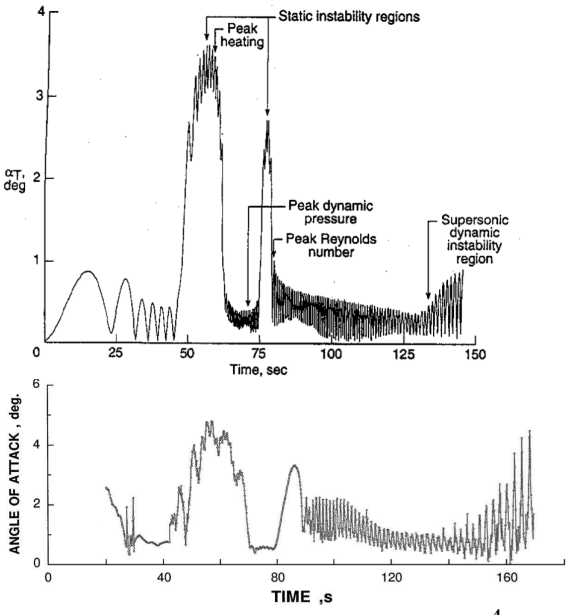

Figure 8. Mars Pathfinder simulated (top[4]) and reconstructed (bottom[5]) angle-of-attack history. The supersonic dynamic instability develops near Mach 2.5.

B. Nominal Results

The oscillation growth that results from dynamic instability is undesirable for many reasons, but this analysis is concerned only with parachute deployment conditions. High angle-of-attack parachute deployments are dangerous due to the risk of suspension line entanglement and unequal loading during the snatch force generated at line stretch. Past missions to Mars have employed strict requirements on the angle-of-attack at parachute deployment to mitigate the risk of deployment failure. Mars Phoenix, the most recent successful entry vehicle sent to Mars, restricted the parachute deployment to angles-of-attack no greater than ±10º.[27] This analysis uses the Mach number at which the SIAD-augmented aeroshell first exceeds ±10º angle-of-attack ($M_{\alpha=10^\circ}$) as a figure of merit for comparing the isotensoid and tension cone SIAD configurations.

It is useful to analyze the angle-of-attack solution governed by Eq. 5 for expected trends as the aerodynamic parameters are changed. Some physical intuition of the expected non-linear behavior comes from interpreting Eq. 5 as a linear second-order harmonic oscillator, commonly expressed in terms of the damping ratio (ζ) and undamped natural frequency (ω_n):

$$\ddot{\alpha} + 2\zeta\omega_n\dot{\alpha} + \omega_n^2\alpha = 0 \tag{15}$$

It is evident that the terms of B (Equation 6a) dictate the pitch-damping behavior, and the terms of C (Equation 6b) dictate the pitch oscillation frequency. Thus, we can predict how using a SIAD affects the pitching frequency and damping by examining the aerodynamic terms in Eqs. 6 individually.

Table 4 shows how the pitch frequency and damping are affected by changes to the aerodynamic terms in Eq. 5. The pitching-moment slope coefficient is negative (statically stable) for the sphere-cone and both SIAD configurations. As this term becomes more negative, Eq. 6b shows that oscillation frequency will increase. Recall from Fig. 4 that the static restoring moment is stronger (more negative) for the isotensoid than the tension cone, so the isotensoid may oscillate at a slightly higher frequency. The second row in Table 4 describes the effect of the pitch-damping sum on the motion. This term shows up in Eq. 6a: notice the pitch-damping sum is multiplied by the square of the reference diameter (shown in the term in Table 4) as well as the reference area itself. As such, the net damping effect is highly dependent on the physical size of the blunt-body. The destabilizing effect of the area increase is weakly countered by the post-inflation increase in pitch-axis mass moment of inertia, I_{yy}. Although deployment moves mass away from the pitch axis, the SIAD's contribution to the net SIAD-aeroshell pitch-axis mass moment of inertia is relatively small. Table 2 and Table 3 show that the change in SIAD-aeroshell I_{yy} from either SIAD configuration's stowed state to the deployed state is less than 10%. In other words, the inertial effect of moving mass away from the pitch axis is negligible compared to the aerodynamic effect of increasing the area exposed to the high-energy flow. Thus, substantial oscillation decay should be expected after SIAD deployment if the pitch-damping sum is negative. Conversely, substantial oscillation growth should be expected after SIAD deployment if the pitch-damping sum is positive. Finally, consider the lift-slope coefficient in Eq. 6a. The damping

contribution from the lift slope (often referred to as the "heave" or "plunge" damping) is generally much smaller than that of the pitch-damping sum. However, for instances where the pitch-damping sum is numerically near zero, the heave damping can have a minor effect on the observed oscillation growth or decay. In a study of shape influence on pitch-dynamics, Dayman[28] verified through computational analyses and experiment that a more negative lift-slope coefficient corresponds to elevated oscillation growth. Although the negative lift-slope coefficients for the tension cone and isotensoid make a minor contribution to the observed oscillation growth, the aerodynamic effect of area increase drives the dynamic behavior by magnifying the pitch-damping sum.

Table 4. General SIAD oscillation frequency and damping trends as aerodynamic parameters are changed.

Term	Direction of Change	Frequency Effect, C	Damping Effect, B
C_{m_α} (static stability)	More negative	Higher frequency oscillation	No effect
$\frac{md^2}{2I_{yy}}\left(C_{m_q}+C_{m_{\dot{\alpha}}}\right)$	More negative	No effect	Substantial oscillation decay
C_{L_α} (heave damping)	More negative	No effect	Minor oscillation growth if pitch-damping sum is zero

Pitch oscillation solutions for trajectories employing the tension cone and isotensoid are shown below in Fig. 9. These nominal results prescribe the MSL pitch-damping behavior shown earlier in Fig. 4. The two solutions are identical prior to SIAD deployment from Mach 6 to Mach 5. The SIAD deployment at Mach 5 greatly exaggerates the amplitude decay relative to the aeroshell-only result in Fig. 7. The mathematical analysis described in Table 4 showed that the isotensoid's stronger static restoring moment results in a higher oscillation frequency. This is evident in the nominal results as the isotensoid is quicker to damp out the initial oscillation from the aeroshell-only portion of flight. At Mach 2.8, the sign of the pitch-damping sum becomes positive and an abrupt growth in oscillation amplitude is evident. The larger reference area of the SIAD-augmented aeroshell greatly increases the magnitude of the damping term (Eq. 6a) in the governing equation (Eq. 5). Furthermore, the amplitude growth occurs faster for the isotensoid than the tension cone due to the isotensoid's higher oscillation frequency. Thus, by assuming MSL pitch damping for the SIAD portion of flight, parachute deployment must occur at a slightly higher Mach number for the isotensoid than the tension cone. The nominal isotensoid and tension cone solutions first exceed 10º angle-of-attack at Mach 2.37 and Mach 2.15, respectively.

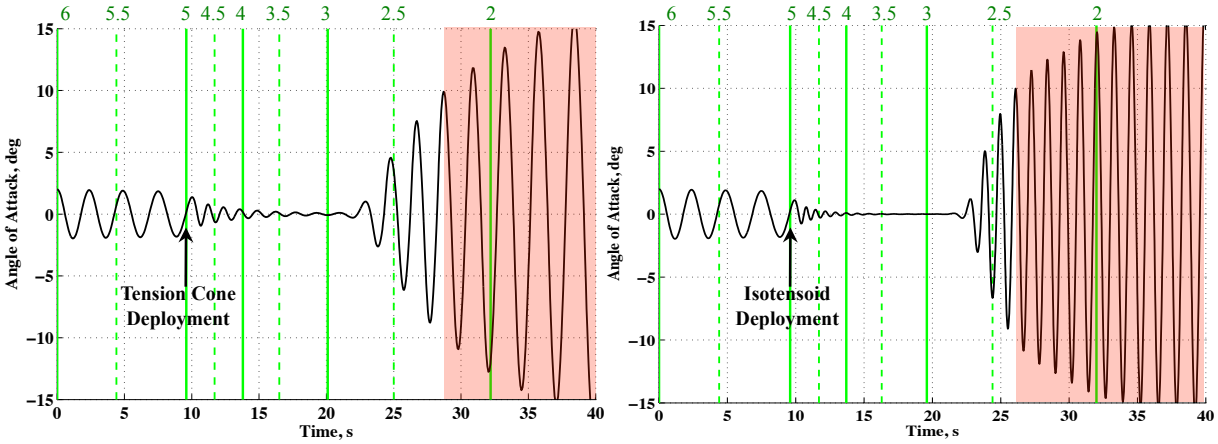

Figure 9. Oscillation of the aeroshell augmented with a tension cone (left) and an isotensoid (right) assuming MSL pitch damping. Vertical lines show Mach number, and the shaded region indicates that α = 10º has been exceeded.

The pitch oscillation solutions in Fig. 9 are based on the hypothetical situation where the SIAD-augmented aeroshell has the same pitch damping as the aeroshell alone. In reality, the flex-interaction mode between the rigid aeroshell and the flexible SIAD that will affect the dynamic stability. This aeroelastic effect has been observed in

wind tunnel tests of flexible isotensoid and tension cone articles. Tanner[3] observed that the isotensoid tends to remain aligned with the freestream flow direction when operating at an angle-of-attack. In contrast, the tension cone tends to remain mostly aligned with the sting when operating at angle-of-attack.[2,3] The flex-interaction mode observed in these static aeroelastic tests is expected to be evident in future wind tunnel tests of an oscillating SIAD-aeroshell test article.

C. Parameterized Pitch-damping Results

The nominal results show that measurement of the pitch-damping characteristics of the SIAD-augmented aeroshell is an important prerequisite for determining safe operating regimes for this decelerator technology. In a dynamic stability analysis that modeled an isotensoid and aeroshell as mechanically attached rigid bodies, Axdahl[10] suggests that the flex-interaction mode may provide a stabilizing effect relative to a completely rigid aeroshell. Thus, the parameterized pitch-damping results discussed here serve as a tool for mission designers wishing to assess the system-level implications of a future dynamic stability data set that captures the flex-interaction mode. The functional form of the pitch-damping sum is assumed to be the same as that of the MSL ballistic range results shown in Figure 4. The pitch-damping sum is parameterized in four different ways in order to assess the sensitivity of 10º angle-of-attack Mach number ($M_{\alpha=10^\circ}$) to potential dynamic stability test results.

The MSL pitch-damping results show an abrupt change to dynamically unstable aerodynamics near Mach 2.8. The magnitude of the pitch-damping sum at zero angle-of-attack changes from a dynamically stable value of -0.46 to a dynamically instable value of 2.7 resulting in the undesirable oscillation amplitude growth shown in Fig. 9. This parameterization method examines the sensitivity of the 10º angle-of-attack Mach number to the maximum value of the pitch-damping coefficient, $C_{mq,max}$. Results are shown below in Fig. 10 with an example of a truncated pitch-damping coefficient Mach-α space. As expected, it is possible to fly unassisted by a stabilizing parachute to lower Mach numbers if $C_{mq,max}$ is reduced. Little benefit is seen for values of $C_{mq,max}$ greater than 1.5, but further $C_{mq,max}$ reduction yields 10º angle-of-attack Mach numbers into the low supersonic to subsonic regimes. In a computational analysis of SIAD dynamic stability, Murman predicted a value of $C_{mq,max}$ = 0.18 for a rigid tension cone (occurs at Mach 2.5). If this result holds true for a flexible tension cone, then the parameterization suggests the tension cone will not exceed 10º angle-of-attack until subsonic speeds. Note that the tension cone always reaches 10º angle-of-attack at a lower Mach number than the isotensoid in these parameterized results. As discussed in the nominal results, this is an artifact of the isotensoid's stronger static restoring moment and thus higher oscillation frequency. Assuming that both SIADs have the same pitch-damping behavior, both SIADS will reach 10º angle-of-attack in a similar number of cycles. Since the isotensoid has a higher oscillation frequency than the tension cone, an angle-of-attack of 10º is reached in a shorter period of time.

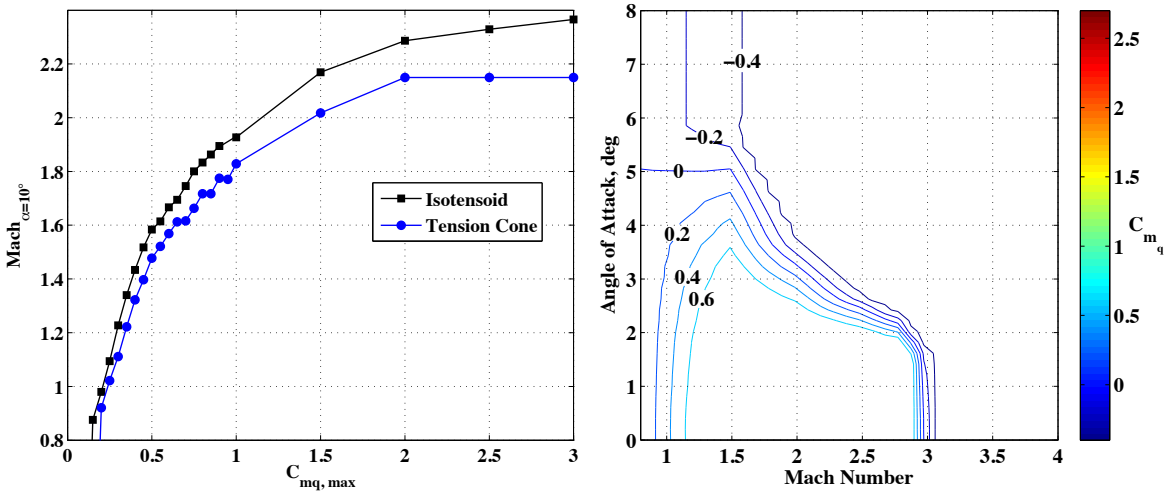

Figure 10. Effect of capping MSL pitch-damping coefficient at a value $C_{mq,max}$ (left), shown with an example of the pitch-damping truncation for $C_{mq,max}$ = 0.6 (right).

Three other pitch-damping parameterization methods are explored in order to encompass a range of potential test data. Figure 11 shows the effect of linearly scaling the pitch-damping coefficient according to Eq. (16) below:

$$\left(C_{m_q}\right)_{SIAD} = \lambda\left(C_{m_q}\right)_{MSL} \tag{16}$$

where λ is a pitch-damping scale factor. Equation 16 yields the nominal results when λ = 1 and neutral pitch damping when λ = 0. Note that this scale-factor parameterization method also reduces the magnitude of the favorable pitch damping (in the example shown in Fig. 11, the high Mach number pitch-damping coefficient of -0.4 is reduced to -0.2). The similarity of these results to those in Fig. 10 shows that the dynamically unstable region of the pitch-damping space is much more influential on the behavior than the dynamically stable region. In other words, experimental aerodynamicists should focus on testing where transition to dynamic instability may occur rather than trying to achieve measurements in the dynamically stable regimes. Understanding where the dynamic instability transition will occur is more valuable than knowledge of the pitch damping within a stable Mach-α space.

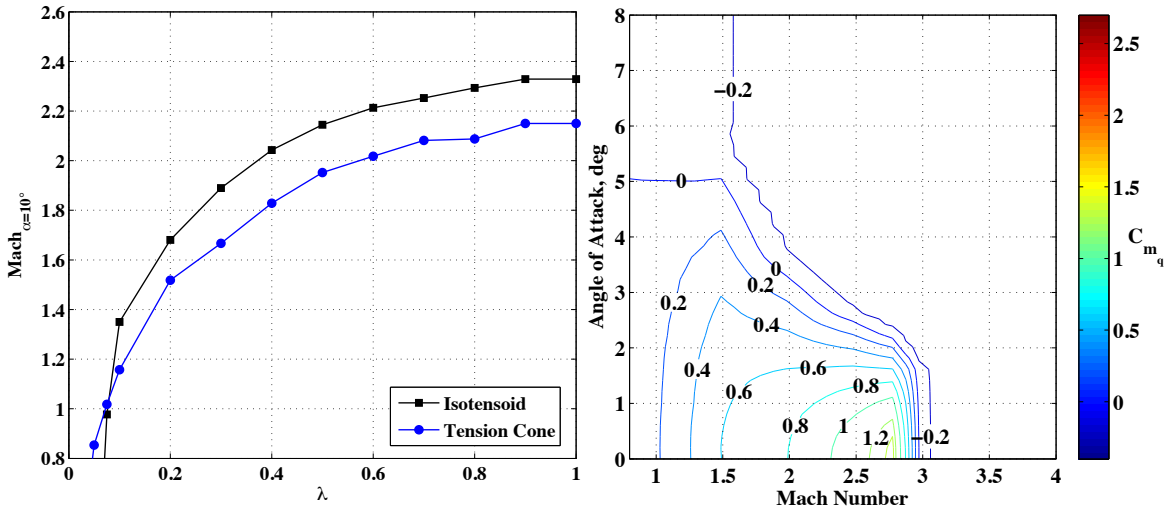

Figure 11. Effect of scaling MSL pitch-damping coefficient according to Eq. (16) (left), shown with example an example of the pitch-damping scaling for λ = 0.5 (right).

Two additional parameterization techniques do not truncate or scale the MSL pitch-damping coefficient, but instead opt to shift the nominal behavior in the Mach-α space. Of particular interest is the effect of shifting the Mach number at which at the dynamic instability develops from the nominal value of Mach 2.8 to a lower speed. Fig. 12 shows the effect of shifting the MSL pitch-damping coefficient by an increment $\Delta Mach$. Not unexpectedly, the value of $M_{\alpha=10^\circ}$ decreases from the nominal condition ($\Delta Mach$ = 0) by an amount very near $\Delta Mach$. Recall from the nominal results in Fig. 9 that the pitch oscillation is almost completely damped out prior to the pitch-damping sign reversal at Mach 2.8, so any extra time spent in the dynamically stable regime cannot make the pre-deployment oscillation amplitude any more favorable for SIAD deployment. Finally, Fig. 13 shows the effect of shifting the MSL pitch-damping coefficient by an angle-of-attack increment $\Delta\alpha$. This has the effect of removing the largest dynamic instabilities that occur at zero angle-of-attack, and thus larger values of $\Delta\alpha$ correspond to lower values of $M_{\alpha=10^\circ}$.

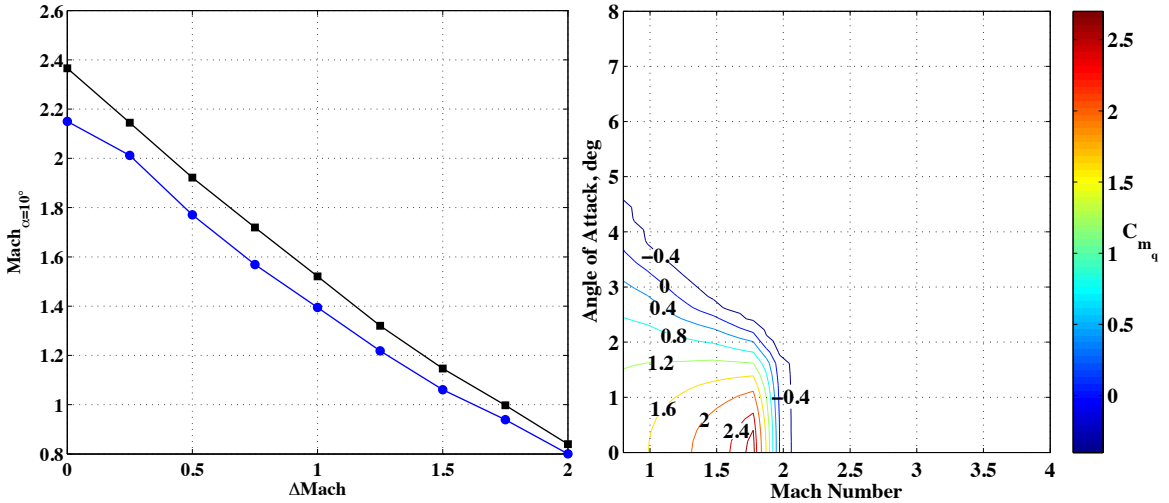

Figure 12. Effect of shifting MSL pitch-damping coefficient by an increment ΔMach (left), shown with example an example of the pitch-damping shift for ΔMach = 1.0 (right).

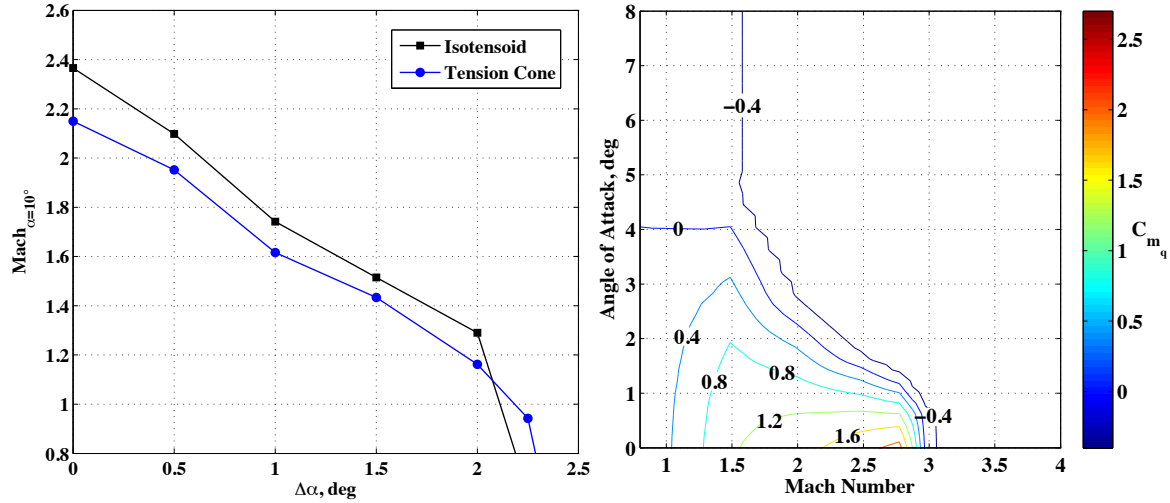

Figure 13. Effect of shifting MSL pitch-damping coefficient by an increment $\Delta\alpha$ (left), shown with example an example of the pitch-damping shift for $\Delta\alpha$ = 1.0° (right).

This analysis is anchored in well-informed blunt-body dynamic stability data by assuming that the isotensoid and tension cone pitch dynamics take the same functional form as the MSL ballistic range results. The parameterized pitch-damping results shown in Figs. 10-13 provide a tool for quickly assessing the system-level implications of SIAD-aeroshell dynamic stability test data. The lower-limit Mach number for parachute deployment can be quickly estimated and trajectory analyses adjusted accordingly. It is evident that future SIAD-aeroshell dynamic stability data has the potential to impose speed restrictions that fundamentally modify the EDL scheme. The isotensoid and tension cone have strikingly different static aeroelastic behavior, and the relative stiffness of the SIAD-aeroshell interface plays an important role in the overall dynamic stability[10]. Furthermore, it has already been noted that the aftbody geometry, an important factor in dynamic stability, is quite different for the isotensoid and tension cone. This analysis shows that such tests may reveal that one SIAD configuration can safely operate at lower Mach numbers than the other and could provide an important discriminator for configuration down-selection.

D. SIAD Dynamic Stability Ground Test Challenges

This analysis shows the importance of obtaining dynamic stability data for the isotensoid and tension cone SIAD configurations. Measuring the dynamic stability of blunt bodies remains a challenging area of research. The

measurement difficulty stems from a few main sources of trouble: a general lack of knowledge regarding the fundamental wake-flow physics driving the oscillation, the inherent support interference effects introduced with current wind tunnel test methods, and the subjectivity introduced in data reduction. Experimentalists have had adequate success measuring dynamic stability of lifting vehicles like fighter aircraft using wind tunnel test techniques such as free- or forced-oscillation. In free-oscillation, the vehicle is supported on an aft-mounted sting or a transverse rod and is allowed to rotate freely. Parameter estimation methods employ the captured pitch angle history to back out the stability derivatives. In forced-oscillation, a controllable sting moves the vehicle through prescribed pitch-angle amplitudes at or near the vehicle's resonant frequency. The moment required to maintain the motion is measured and the damping coefficients are computed directly rather than inferred from the oscillation history.[29] Unlike static aerodynamic tests where sting effects are often not influential on the measured quantities, support interference can fundamentally change the results of a dynamic tests. Relative motion between the model and support influences the static pitching moment, and the phase relationship used to relate the static pitching moment and pitch-damping sum is severely distorted.[30] Despite this unfortunate reality, both free- and forced-oscillation methods work reasonably well for aircraft because the damping quantity being measured is a dominant factor in the observed motion and wake flow effects are not as important for these geometries. However, the damping derivatives of blunt entry vehicles are much more subtle than for fighter aircraft, and the dynamic data is even more susceptible to corruption from sting interference effects. As a result, the American Mars entry vehicles have relied heavily on free-flight dynamic stability data taken in ballistic range tests.[26,18,7]

A ballistic range can provide the most flight-like environment for supersonic and transonic dynamic stability testing. In this method, high-strength dynamically scaled models are loaded in a gun barrel, or sabot, and launched through the range with enormous acceleration on the order of 10^6g.[31] The primary advantage of this technique is that a sting is not necessary to support the model's oscillation, so a dynamically scaled model will mimic the behavior seen in flight. It was discussed earlier that ballistic range tests, while replicating the flight environment, present a challenge to engineers reducing the observed motion into aerodynamic coefficients. Orthogonal shadowgraphs taken at multiple stations along the flight path provide orientation tracking. The inferred pitch-damping coefficients are a function of the technique used to translate discrete position data from the imagery into the coefficients of the non-linear pitch-damping equation (Eq. 4), and although the two companies that reduced the MSL ballistic range data estimated different functional forms for the pitch damping, the integrated effect of both data sets match the observed oscillations well.[7] Engineers seeking to measure blunt-body dynamic stability have been well served by ballistic range methods, especially considering the shortcomings of the alternative wind tunnel methods. However, SIADs introduce the additional complexity of flexibility. This analysis and others have speculated that the flex-interaction mode between the rigid aeroshell and flexible SIAD could drive the dynamic stability. Ballistic range tests, traditionally requiring rigid models due to the enormous loads at sabot firing, may not be able to provide relevant data for flexible structures.

The necessity to capture the SIAD-aeroshell flex-interaction during dynamic stability testing suggests that free- or forced-oscillation testing may be required to obtain relevant data. The challenge will be to design a test setup where a sting can attach to the test article through the center of gravity without significantly altering the static aerodynamics and wake flow. Quantitative free-oscillation measurements may not be possible for some conditions where the model is dynamically unstable because the pitch angle could be amplified beyond the design limits of the test equipment. Engineers at NASA Langley recently had success obtaining transonic dynamic stability data for CEV using the forced-oscillation technique by employing a transverse sting through the center of gravity.[7] Equipment and expertise from this test series should be leveraged if any future SIAD forced-oscillation tests are planned. In order to make the best use of resources, the testing strategy should focus on identifying the Mach number at which dynamic stabilities begin to develop. Research efforts will be better focused if mission designers communicate a nominal parachute deployment Mach number to the dynamic stability test planning personnel. Using this Mach number as a starting point, a test plan should be formulated that obtains dynamic stability data at progressively higher Mach numbers until dynamic stability is observed. If the SIAD-augmented aeroshell is dynamically stable at the nominal parachute deployment Mach number then further testing may not be necessary. Blunt-bodies tend to be more dynamically stable at progressively higher Mach numbers, and this analysis has showed that pitch oscillations of a dynamically stable SIAD-augmented aeroshell are highly damped.

IV. Conclusion

Near-term missions to Mars may not be possible with heritage deployable decelerator technology. Through static wind tunnel testing and computational analyses, the attached isotensoid and tension cone SIADs have proven themselves as formidable alternatives to Viking-era technology that have the potential to provide the needed drag

performance at far more severe flight conditions. A key open question remains: how does the SIAD behave dynamically as the vehicle decelerates into low supersonic speeds where blunt-bodies are traditionally unstable? By the time the vehicle has decelerated enough to permit subsonic or supersonic parachute deployment, the amplitude of oscillation may be too large to permit safe deployment. This analysis considers the dynamic impact of outfitting a candidate Mars 2018 aeroshell with an attached isotensoid or tension cone SIAD deployed at Mach 5. Only oscillatory motion in the pitch-plane below Mach 6 is considered. The equations governing the ballistic trajectory and pitch dynamics are solved numerically. Static aerodynamic force coefficients are taken from a comprehensive experimental database of flexible SIAD models. Since the pitch-damping coefficients for the tension cone and isotensoid have not been measured, a parameterization technique is employed to capture the main effects of the SIAD pitch damping on the observed oscillation. In particular, it is assumed that both SIADs will have pitch-damping coefficients of the same functional form as results from the MSL ballistic range tests. Results from the parameterization technique can be used as a tool for quick assessment of the system-level implications of dynamic stability results.

Using parachute deployment requirements from the Mars Phoenix lander mission, the pitch-damping behavior yielding unacceptable oscillation amplitude growth is quantified. The numerical scheme used to solve the governing equations is validated using a known analytical solution to a simplified problem. The aerodynamic terms in the pitch-oscillation equation are evaluated for their contribution to the damping behavior in order to help interpret results from simulation experiment. Nominal results, where MSL pitch damping is applied without modification to the SIAD portion of flight, suggest that the isotensoid and tension cone will reach undesirable oscillation amplitudes at Mach 2.37 and Mach 2.15, respectively. Although any pre-deployment oscillations are quickly damped out at SIAD inflation due to the magnification of the favorable pitch damping at Mach 5, blunt-body dynamic stability inevitably deteriorates as the vehicle decelerates to lower Mach numbers. Various parameterizations of the pitch-damping Mach-α space reveal certain conditions where deceleration is possible all the way to subsonic conditions before the pitch amplitude is prohibitively large. This analysis is complemented by past work showing that the flex-interaction mode between the flexible SIAD and the rigid aeroshell has the potential to improve dynamic stability.

Experimental identification of blunt-body pitch-damping behavior remains a challenging task. Current test methods either rely on parameter estimation techniques to compute non-unique aerodynamic coefficients from free-flight data or rely on data measured in a wind tunnel that is subject to corruption from support interference. Past missions to Mars have all used pitch-damping data reduced from ballistic range tests because it is the most representative of free-flight behavior. Flexibility introduced by employing SIAD technology may preclude the use of a ballistic range, where models are normally dynamically scaled using solid metal pieces in order to survive the enormous loads encountered at sabot ejection. Dynamic testing of SIAD-augmented aeroshell models may only be feasible using support-mounted models in a wind tunnel. Free- and forced-oscillation test methods have been used widely in the past to measure pitch damping of aircraft but are rarely used for for blunt vehicles. The challenge is to design a test support that minimizes corruption of the static aerodynamics without polluting the wake flow. Given the potential difficulty and cost of obtaining SIAD dynamic stability data at all a wide range of Mach numbers, a testing strategy is recommended that focuses on identifying flight conditions where dynamic instabilities first develop.

Acknowledgments

The authors wish to acknowledge Tom Rivellini and George Chen of NASA Jet Propulsion Laboratory, Mark Schoenenberger and Chuck Player of NASA Langley Research Center, and Chris Tanner and Jeremy Hill of the Georgia Tech Space Systems Design Laboratory for their support and advice.

References

[1]Clark, I.G., Hutchings, A.L., Tanner, C.L., Braun, R.D., "Supersonic Inflatable Aerodynamic Decelerators for Use on Future Robotic Missions to Mars," *Journal of Spacecraft and Rockets*, Vol. 46, No. 2, 2009, pp. 340-352.

[2]Clark I.G., "Aerodynamic Design, Analysis, and Validation of a Supersonic Inflatable Decelerator," Ph.D. Dissertation, Daniel Guggenheim School of Aerospace Engineering, Georgia Institute of Technology, Atlanta, GA, 2009.

[3]Tanner, C.L., Cruz, J.R., Hughes, M.F., Clark, I.G., Braun, R.D., "Subsonic and Transonic Wind Tunnel Testing of Two Inflatable Aerodynamic Decelerators," *7th International Planetary Probe Workshop*, Barcelona, Spain, 2010.

[4]Braun, R.D., Powell, R.W., Engelund, W.C., Gnoffo, P.A., "Mars Pathfinder Six-Degree-of-Freedom Entry Analysis," *Journal of Spacecraft and Rockets*, Vol. 32, No. 6, 1995, pp. 993-1000.

[5]Spencer, D.A., Blanchard, R.C., Braun, R.D., Kallemeyn, P.H., Thurman, S.W., "Mars Pathfinder Entry, Descent, and Landing Reconstruction," *Journal of Spacecraft and Rockets*, Vol. 36, No. 3, 1999, pp. 357-366.

[6]Mitcheltree, R.A., Fremaux, C.M., Yates, L.A., "Subsonic Static and Dynamic Aerodynamics of Blunt Entry Vehicles," *37th AIAA Aerospace Sciences Meeting and Exhibit*, 1999-1020, AIAA, Washington, DC, 1999.

[7]Schoenenberer, M., Yates, L., Hathaway, W., "Dynamic Stability Testing of the Mars Science Laboratory Entry Capsule," *41st AIAA Thermophysics Conference*, 2009-3917, AIAA, Washington, DC, 2009.

[8]Musil, J.L., "Study of Expandable Terminal Decelerators for Mars Atmosphere Entry, Volume I – Final Summary Report," Goodyear Aerospace Corporation, Rept. GER-12842, Akron, OH, Oct. 1966.

[9]Musil, J.L., "Study of Expandable Terminal Decelerators for Mars Atmosphere Entry, Volume II – Supporting Data and Technical Analysis," Goodyear Aerospace Corporation, Rept. GER-12842, Akron, OH, Oct. 1966.

[10]Axdahl, E., Cruz, J.R., Schoenenberger, M., Wilhite, A., "Flight Dynamics of an Aeroshell Using an Attached Inflatable Aerodynamic Decelerator," *AIAA Aerodynamic Decelerator Systems Technology Conference*, 2009-2963, AIAA, Washington, DC, 2009.

[11]Bohon, H.L., Miserentino, R., "Deployment and Performance Characteristics of 5-Foot-Diameter (1.5 m) Attached Inflatable Decelerators From Mach Number 2.2 to 4.4," NASA TN D-5840, 1970.

[12]Bohon, H.L., Sawyer, J.W., "Deployment and Performance Characteristics of 1.5-Meter Supersonic Attached Inflatable Decelerators," NASA TN D-7550, 1974.

[13]Mikulas Jr., M.M., Bohon, H.L., "Development Status of Attached Inflatable Decelerators," *Journal of Spacecraft*, Vol. 5, No. 6, 1969, pp. 654-660.

[14]Regan, F.J., and Anandakrishnan, S.M., *Dynamics of Atmospheric Re-Entry*, AIAA Education Series, AIAA, Washington, DC, 1993, pp. 179-222, 369-424.

[15]Schoenenberger, M., Queen, E.M., Litton, D., "Oscillation Amplitude Growth for a Decelerating Object with Constant Pitch Damping," *AIAA Atmospheric Flight Mechanics Conference and Exhibit*, 2006-6147, AIAA, Washington, DC, 2006.

[16]Tannehill, J.C., Anderson, D.A., Pletcher, R.H., *Computational Fluid Mechanics and Heat Transfer*, 2nd ed., Taylor & Francis, Philadelphia, 1997, Chap. 3.

[17]Grant, M.J., Braun, R.D., "Analytic Hypersonic Aerodynamics for Conceptual Design of Entry Vehicles," *48th AIAA Aerospace Sciences Meeting*, 2010-1212, AIAA, Washington, DC, 2010.

[18]Schoenenberger, M., Hathaway, W., Yates, L., Desai, P., "Ballistic Range Testing of the Mars Exploration Rover Entry Capsule," *AIAA Aerospace Sciences Meeting and Exhibit*, 2005-55, AIAA, Washington, DC, 2005.

[19]Hill, J., "An Experimental Static Aerodynamics Database for Trajectory Analysis of Supersonic Inflatable Aerodynamic Decelerators," *AIAA Aerodynamic Decelerator Systems Technology Conference*, Pending Publication, AIAA, Washington, DC, 2009.

[20]Hirschel, E.H., Weiland, C., *Selected Aerothermodynamic Design Problems of Hypersonic Flight Vehicles*, Springer-Verlag, Berlin, 2009.

[21]Winchenbach, G.L., Chapman, G.T., Hathaway, W.H., Ramsey, A., Berner, C., "Dynamic Stability of Blunt Atmospheric Entry Configurations," *Journal of Spacecraft and Rockets*, Vol. 39, No. 1, 2002, pp. 49-55.

[22]Murman, S.M., "Dynamic Simulations of Atmospheric-Entry Capsules," *Journal of spacecraft and Rockets*, Vol. 46, No. 4, 2009, pp. 829-835.

[23]Murman, S.M., "Dynamic Simulations of Inflatable Aerodynamic Decelerator Concepts," *AIAA Aerodynamic Decelerator Systems Technology Conference*, 2009-2964, AIAA, Washington, DC, 2009.

[24]Ludlow, D.K., Qin, N., "Computational Prediction of Pitch Damping for High Mach Number Blunt Projectiles," AIAA-98-0394, AIAA, Washington, DC, 1998.

[25]Platzer, M.F., Sherer, A.D., "Dynamic Stability Analysis of Bodies of Revolution in Supersonic Flow," *Journal of Spacecraft*, Vol. 5, No. 7, 2009, pp. 833-837.

[26]Sammonds, R.I., Kruse, R.L., "Viking Entry Vehicle Aerodynamics at M = 2 in Air and Some Preliminary Test Data for Flight in CO_2 at M = 11," NASA TN D-7974, June 1975.

[27]Edquist, K.T., Desai, P., Schoenenberger, M., "Aerodynamics for the Mars Phoenix Entry Capsule," AIAA 2008-7219, AIAA, Washington, DC, 2008.

[28]Dayman Jr., B., Brayshaw Jr., J.M., Nelson, D.A., Jaffe, D.A., Babineaux, T.L., "The Influence of Shape on Aerodynamic Damping of Oscillatory Motion during Mars Atmosphere Entry and Measurement of Pitch Damping at Large Oscillation Amplitudes," Jet Propulsion Laboratory Technical Report No. 32-380, 1963.

[29]Schueler, C.J., Ward, L.K., Hodapp Jr., A.E., "Techniques for Measurement of Dynamic Stability Derivatives in Ground Test Facilities," NATO Advisory Group for Aerospace Research and Development, Rept. 121, 1967.

[30]Ericsson, L.E., Reding, J.P, "Review of Support Interference in Dynamic Tests," *AIAA Journal*, Vol. 21, No. 12, 1983, pp. 1652-1666.

[31]Canning, T.N., Seiff, A., James, C.S., "Ballistic-Range Technology," NASA Advisory Group for Aerospace Research and Development, Rept. 138, 1970.